Study of charge density waves in suspended 2H-TaS_2 and 2H-$TaSe_2$ by nanomechanical resonance

Lee, Martin; Šiškins, Makars; Mañas-Valero, Samuel; Coronado, Eugenio; Steeneken, Peter G.; van der Zant, Herre S.J.

DOI
10.1063/5.0051112

Publication date
2021

Document Version
Final published version

Published in
Applied Physics Letters

Applied Physics Letters

Study of charge density waves in suspended 2H-TaS_2 and 2H-$TaSe_2$ by nanomechanical resonance

Cite as: Appl. Phys. Lett. **118**, 193105 (2021); https://doi.org/10.1063/5.0051112
Submitted: 22 March 2021 • Accepted: 26 April 2021 • Published Online: 13 May 2021

Martin Lee, Makars Šiškins, Samuel Mañas-Valero, et al.

Applied Physics Letters ARTICLE scitation.org/journal/apl

Study of charge density waves in suspended 2H-TaS_2 and 2H-$TaSe_2$ by nanomechanical resonance

Cite as: Appl. Phys. Lett. **118**, 193105 (2021); doi: 10.1063/5.0051112
Submitted: 22 March 2021 · Accepted: 26 April 2021 ·
Published Online: 13 May 2021

View Online Export Citation CrossMark

Martin Lee,[1,a)] Makars Šiškins,[1] Samuel Mañas-Valero,[2] Eugenio Coronado,[2] Peter G. Steeneken,[1,3] and Herre S. J. van der Zant[1]

AFFILIATIONS

[1]Kavli Institute of Nanoscience, Delft University of Technology, Lorentzweg 1, 2628 CJ Delft, The Netherlands
[2]Instituto de Ciencia Molecular (ICMol), Universitat de València, c/Catedrático José Beltrán 2, 46980 Paterna, Spain
[3]Department of Precision and Microsystems Engineering, Delft University of Technology, Mekelweg 2, 2628 CD Delft, The Netherlands

Note: This paper is part of the APL Special Collection on Charge-Density-Wave Quantum Materials and Devices.
[a)]**Author to whom correspondence should be addressed:** M.Lee-2@tudelft.nl

ABSTRACT

The charge density wave (CDW) state in van der Waals systems shows interesting scaling phenomena as the number of layers can significantly affect the CDW transition temperature, T_{CDW}. However, it is often difficult to use conventional methods to study the phase transition in these systems due to their small size and sensitivity to degradation. Degradation is an important parameter, which has been shown to greatly influence the superconductivity in layered systems. Since the CDW state competes with the onset of superconductivity, it is expected that T_{CDW} will also be affected by the degradation. Here, we probe the CDW phase transition by the mechanical resonances of suspended 2H-TaS_2 and 2H-$TaSe_2$ membranes and study the effect of disorder on the CDW state. Pristine flakes show the transition near the reported values of 75 K and 122 K, respectively. We then study the effect of degradation on 2H-TaS_2, which displays an enhancement of T_{CDW} up to 129 K after degradation in ambient air. Finally, we study a sample with local degradation and observe that multiple phase transitions occur at 87 K, 103 K, and 118 K with a hysteresis in temperature in the same membrane. The observed spatial variations in the Raman spectra suggest that variations in crystal structure cause domains with different transition temperatures, which could result in the hysteresis. This work shows the potential of using nanomechanical resonance to characterize the CDW in suspended 2D materials and demonstrates that the degradation can have a large effect on transition temperatures.

The charge density wave (CDW) state in van der Waals (vdW) materials has recently become a resurgent area of research. Archetypal systems such as 2H-$NbSe_2$, 2H-TaS_2, and 2H-$TaSe_2$ have been under study since the 1970s.[1–14] However, recent works on surprising and unexpected layer dependence and degradation effects on superconductivity (SC) and CDW in these systems have revived interest in studying their phase transitions. For example, the superconducting transition temperature T_{SC} of 2H-$NbSe_2$ is decreased from 7.2 K in the bulk to 3 K in the monolayer limit, while the CDW transition temperature T_{CDW} is increased[15] from 33 K to 145 K. More surprisingly, the 2H-TaS_2 has a T_{SC} of 0.6 K in the bulk which increases to 3 K in a monolayer[16,17] and a T_{CDW} of 75 K which also increases to 140 K.[18] Similar scaling is seen for T_{SC} in 2H-$TaSe_2$.[19] Furthermore, the degradation of the crystal in air has shown to enhance the superconductivity in 2H-TaS_2,[20] which is in stark contrast to other air-sensitive vdW superconductors which lose their superconductivity upon degradation.[21–24] It is an ongoing challenge to clarify these contradicting layer dependencies and degradation effects in order to shine light on the competition between CDW and SC in these materials.

The CDW transition, like other first and second order phase transitions, can be described by Landau's theory of phase transitions,[25] where the emergence of charge order gives rise to a sudden change in the specific heat. Using the specific heat anomaly to probe the phase transition is already established in several systems.[6,26–30] However, the

traditional methods of probing the specific heat are nearly impossible to apply on ultrathin exfoliated 2D material flakes. Recent works on using the nanomechanical resonance to extract various phase transitions including structural, magnetic, and electronic phase transitions[31–34] have shown to be an interesting alternative.

In this work, we study the CDW transitions of suspended 2H-TaS_2 and 2H-$TaSe_2$ flakes by tracking the temperature dependence of their nanomechanical resonance frequency. The resonance frequency of suspended pristine 2H-TaS_2 and 2H-$TaSe_2$ flakes shows an anomaly at the phase transition temperatures of 75 K and 122 K, respectively. We then employ this technique as a probe to study the effect of degradation on the T_{CDW} of 2H-TaS_2. Flakes of 2H-TaS_2 show greatly enhanced T_{CDW} after being exposed to ambient conditions for prolonged durations. Furthermore, we induce local disorder in a region of a suspended part of the membrane, which causes varying degrees of disorder across the flake as observed in Raman spectroscopy. In this sample, multiple transitions appear with a hysteretic switching behavior pointing toward the existence of domains with varying T_{CDW}.

The interferometry setup and the sample are described in Fig. 1. Figure 1(a) shows an illustration of the interferometry setup. The intensity of the blue diode laser ($\lambda_{Blue} = 405$ nm) is modulated by the vector network analyzer (VNA), which optothermally excites the membrane into motion. Simultaneously, a continuous He-Ne laser ($\lambda_{Red} = 632$ nm) is used to readout the movement of the membrane.

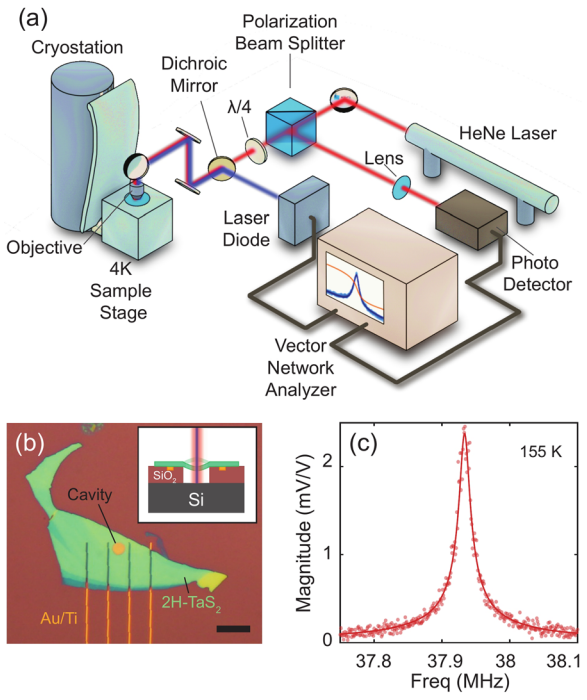

FIG. 1. Interferometry setup, device geometry, and basic characterization of a 2H-TaS_2 membrane. (a) Illustration of the laser interferometry setup. The blue diode laser is used to optothermally actuate the membrane, while the He-Ne red laser is used to readout its motion. (b) Optical image of device 1 composed of a 2H-TaS_2 flake of thickness $t = 31.2 \pm 0.6$ nm transferred onto pre-defined electrodes surrounding a cavity. Scale bar: 10 μm. Inset: Illustration of the cross section of a device. (c) Example frequency response of device 1 at 155 K.

The interference signal is collected by the photodetector which is readout by the VNA. The sample is situated in a 4 K dry cryostat at high vacuum with a heater beneath the sample to control the temperature.

Devices are fabricated by deterministically stamping[35] 2H-TaS_2 and 2H-$TaSe_2$ flakes on top of electrodes metalized by evaporation and circular cavities etched into SiO_2/Si by reactive ion etching. The suspended membrane is in a drum geometry with a rigid Si back mirror. High-quality 2H-TaS_2 and 2H-$TaSe_2$ flakes are exfoliated from synthetically grown bulk crystals.[17,36] Detailed description of the setup and the fabrication processes can be found in the supplementary material.

An optical image of device 1 is shown in Fig. 1(b), the cross-sectional illustration is in the inset, and its typical frequency response at 155 K near the fundamental resonance frequency is in Fig. 1(c). The data are collected at every temperature once stabilized to within 10 mK from the set-point and fitted to a simple harmonic oscillator model. The fundamental resonance frequency $f_0(T)$ extracted from such sweeps is plotted in frequency vs temperature plots in subsequent figures.

In this paragraph, we introduce the lambda-type anomaly in the specific heat due to the normal—CDW phase transition, as described by Landau–Lifshitz.[25,31,37] The Landau free energy can be written for CDW transitions as

$$F = F_0 + a(T - T_{CDW})Q^2 + BQ^4, \tag{1}$$

where F_0 is the temperature-dependent free energy of the normal state, Q is the order parameter, and a and B are phenomenological positive constants. Minimizing the above equation with respect to Q (i.e., $\partial F/\partial Q = 0$) gives the CDW order parameter,

$$Q = \sqrt{\frac{-a(T - T_{CDW})}{2B}}, \tag{2}$$

and a minimum free energy $F_{min} = F_0 - \frac{a^2}{4B}(T - T_{CDW})^2$. Using the relation for the specific heat at constant pressure, $c_p(T) = -T\left[\frac{\partial^2 F}{\partial T^2}\right]_p$ and by substituting the expression for F_{min} into Eq. (1), the magnitude of the jump in the specific heat at the phase transition can be derived as $\Delta c_p = \frac{a^2 T_{CDW}}{2B}$. To find the relationship between the membrane resonance frequency and $c_p(T)$, we note that the fundamental resonance frequency of a circular membrane under thermal strain can be described by

$$f_0(T) = \frac{2.4048}{\pi d}\sqrt{\frac{E}{\rho}\frac{\varepsilon(T)}{(1-\nu)}}, \tag{3}$$

where d is the membrane diameter, E is the Young's modulus, ρ is the density, $\varepsilon(T)$ is the temperature-dependent biaxial strain, and ν is the Poisson's ratio.

The thermal strain accumulated in the membrane is a result of the difference in the linear thermal expansion coefficient of the membrane α_L and that of the substrate α_{Si}. It can be expressed as $\frac{d\varepsilon(T)}{dT} \simeq -(\alpha_L(T) - \alpha_{Si}(T))$, assuming that the thermal expansion coefficient of SiO_2 is negligible in comparison to Si.[38,39] Using the thermodynamic relation between the thermal expansion coefficient and the specific heat, $\alpha_L(T) = \gamma c_v(T)/(3KV_M)$, and the above-mentioned thermal strain relation, we arrive at an expression,

$$c_v(T) = 3\left(\alpha_{si} - \frac{1}{\mu^2}\frac{d\left[f_0^2(T)\right]}{dT}\right)\frac{KV_M}{\gamma}, \quad (4)$$

where $c_v(T)$ is the specific heat of the membrane at constant volume, $K = \frac{E}{3(1-2\nu)}$ is the bulk modulus, γ is the Grüneisen parameter, $V_M = M/\rho$ is the molar volume of the membrane, and $\mu = \frac{2.4048}{\pi d}\sqrt{\frac{E}{\rho(1-\nu)}}$ is a constant. We note that the Young's modulus E is also slightly temperature dependent and exhibits an anomaly at the phase transition. However, this change is on the order of a percent throughout the temperature range of our experiment.[40] We, therefore, approximate it as a constant and assume the thermal strain to be dominant in determining the frequency changes.[31] Since $c_v \simeq c_p$ in solids, Eq. (4) directly relates the mechanical resonance of the membrane to the specific heat derived using the Landau free energy [Eq. (1)]. Through this relation, we can extract the specific heat from the temperature derivative of f_0^2, and thus the T_{CDW} from determining the discontinuity in the specific heat. Detailed discussion on this relation can be found in Ref. 31 and in the supplementary material S.II.

Temperature-dependent mechanical and electrical responses of pristine flakes of 2H-TaS_2 (left column, device 1, thickness, $t = 31.2 \pm 0.6$ nm, $d = 4\,\mu$m) and 2H-$TaSe_2$ (right column, device 2, $t = 23.3 \pm 0.5$ nm, $d = 10\,\mu$m, device not shown) are shown in Fig. 2. Figures 2(a) and 2(b) show the four-probe resistance (left y-axis, pink) and their derivatives (right y-axis, brown). Dashed black lines are plotted as a visual guide to highlight the deviation of the resistance data from the linear drop. The kink below which the resistance drop deviates from the dashed black line is the CDW transition temperature universally seen in other CDW systems.[41] This can also be seen in the $\frac{dR}{dT}$ as the temperature at which the slope changes. The CDW transition temperatures for 2H-TaS_2 and 2H-$TaSe_2$ by analyzing the $\frac{dR}{dT}$ are 77 K and 122 K, respectively, and are in good agreement with the values in literature.[3]

On the same membranes, the resonance frequency f_0 extracted by fitting a simple harmonic oscillator function to the resonance peak such as in Fig. 1(c) is plotted against temperature in Figs. 2(c) and 2(d) in blue (left y-axis). There is a monotonic increase in the resonance frequency as the sample temperature is lowered, arising from the difference in the thermal expansion coefficient between the membrane and the substrate, thus increasing the tension of the resonator. The temperature derivative of f_0^2 is plotted in green in Figs. 2(c) and 2(d) (right y-axis). Since $c_v \propto \frac{d[f_0^2(T)]}{dT}$ from Eq. (4), the phase transition temperature T_{CDW} can be determined as the temperature where the peak in $\frac{d[f_0^2(T)]}{dT}$ is observed. The T_{CDW} of 2H-TaS_2 and 2H-$TaSe_2$ extracted from Figs. 2(c) and 2(d) is 75 K and 122 K, respectively, and is in good agreement with the values from the transport data as well as the literature values.[3] Therefore, this method can be a complementary tool to the transport technique to probe the phase transition in CDW materials, which show subtle changes in the slope of the resistance. In the subsequent paragraphs, the T_{CDW}s are extracted by finding the peak position of the anomaly in $\frac{d[f_0^2(T)]}{dT}$ vs T.

The $c_v(T)$ can be estimated from the same data by including the material parameters into Eq. (4). The reported material parameters for 2H-TaS_2 are $E = E_{2D}/t = 149$ GPa,[42] assuming an interlayer spacing $t = 0.58$ nm, $\nu = 0.27$,[42] and $\rho = 6110$ kg/m^3. The parameters for 2H-$TaSe_2$ are $E = 120$ GPa,[40] $\nu \sim 0.2$,[43] and $\rho = 8660$ kg/m^3. The

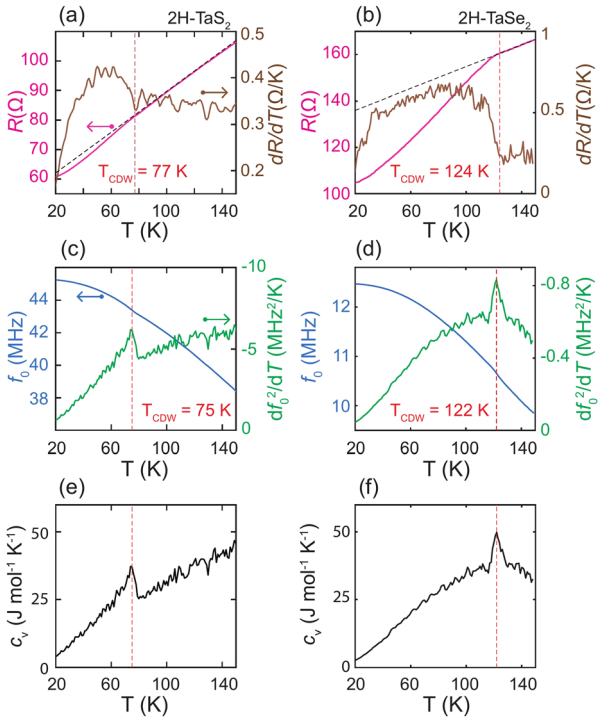

FIG. 2. Electrical and mechanical characterization of a pristine 2H-TaS_2 (left column, device 1) and 2H-$TaSe_2$ (right column, device 2) membrane. Dashed red lines indicate the CDW transition temperature determined from $\frac{dR}{dT}$ and the peak of $\frac{d[f_0^2(T)]}{dT}$. [(a) and (b)] Four-probe resistance as a function of temperature (left y-axis, pink) and its derivative (right y-axis, brown). Dashed straight black lines are plotted as visual aid. [(c) and (d)] Resonance frequency f_0 (left y-axis, blue) and $\frac{d[f_0^2(T)]}{dT}$ (right y-axis, green). [(e) and (f)] Specific heat extracted from [(c) and (d)] using Eq. (4). The data from device 1 are also used in Ref. 31, Šiškins *et al.*, "Magnetic and electronic phase transitions probed by nanomechanical resonators," Nat. Commun. **11**, 2698 (2020). Copyright 2020 Author(s), licensed under a Creative Commons Attribution (CC BY) license.

Grüneisen parameters can be estimated as $\gamma \simeq \frac{3}{2}\left(\frac{1+\nu}{2-3\nu}\right)$.[44] Finally, the temperature-dependent thermal expansion coefficient of single crystalline Si is used as experimentally measured in Ref. 45. Using these parameters, the $\frac{d[f_0^2(T)]}{dT}$ data in Figs. 2(c) and 2(d) are converted to c_v and plotted in Figs. 2(e) and 2(f).

For the remainder of the study, we focus on the effect of degradation on the CDW transition, specifically in 2H-TaS_2. We first use the above-mentioned technique to probe the phase transition temperature in 2H-TaS_2 before and after prolonged exposure to air. Degradation is often accompanied by changes in the material properties such as doping,[20] Poisson's ratio,[46] Young's modulus,[47] dimensions,[48] and density.[49] Therefore, in the following, we extract the transition temperatures from $\frac{d[f_0^2(T)]}{dT}$ plots and refrain from showing c_v in order to circumvent errors in c_v arising from using wrong material parameters in Eq. (4).

To study degradation effects on the CDW transition temperature, device 3 ($t = 53.3 \pm 0.7$ nm, $d = 5\,\mu$m) is measured before and after exposure to ambient conditions. In the first measurement, it is cooled down immediately following fabrication. Figure 3(a) shows f_0 (blue) as

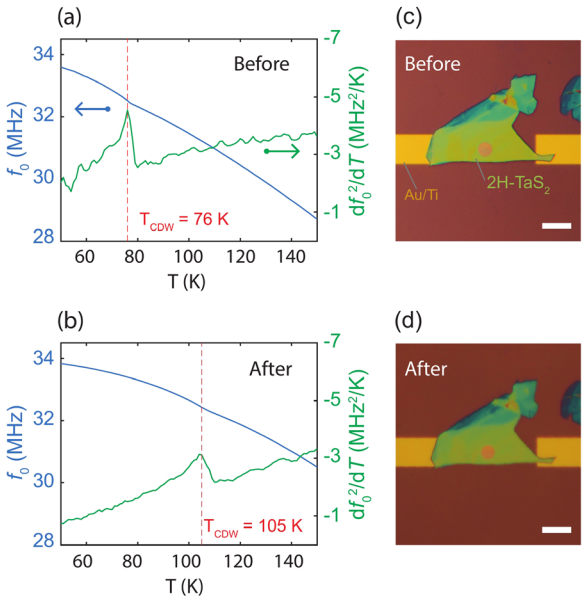

FIG. 3. Enhancement of the T_{CDW} from the pristine state to the degraded state in device 3 (2H-TaS_2). f_0 (blue, left y-axis) and $\frac{d[f_0^2(T)]}{dT}$ (green, right y-axis) measured (a) immediately following fabrication and (b) after exposure to ambient conditions for several hours. Optical image of the device (c) immediately after fabrication and (d) after measurements of [(a) and (b)]. Scale bar: 10 μm. Dashed red lines correspond to the T_{CDW}.

well as the temperature derivative of f_0^2 (green). As expected, the CDW transition occurs at $T_{CDW} = 76$ K (dashed red line), which is in good agreement with device 1 and literature values.[3] After the first cooldown, the sample is removed from the cryostat and is exposed to air for several hours.

In the second cooldown, a remarkable 29 K enhancement of the T_{CDW} is observed. As shown in Fig. 3(b), the anomaly in $\frac{d[f_0^2(T)]}{dT}$ occurs at 105 K instead of 76 K. Several additional samples of air-degraded 2H-TaS_2 have been measured, one of which showed an even higher T_{CDW} of 129 K (see the supplementary material S.III). In contrast to the drastic change in the T_{CDW}, no observable changes in the optical microscopy images before and after could be identified. Figure 3(c) is an image of device 3 immediately after the stamping process, whereas Fig. 3(d) is the image taken after the second round of measurements.

We have also fabricated and measured several different samples of 2H-TaS_2 drums with a disorder created by laser-induced oxidation[50] and focused ion beam (FIB)-induced milling[51] to intentionally degrade the suspended flakes. Neither of these samples with different forms of disorder showed the CDW transition (see the supplementary material S.IV). However, in device 4, an electrostatic discharge across two electrodes adjacent to the suspended membrane caused a severe degradation of the membrane between the two electrodes. Figure 4(a) shows an image of the device immediately after fabrication showing no signs of damage. In Fig. 4(b), a scanning electron microscopy (SEM) image is shown of the device after the measurements are taken. It shows that the discharge caused severe damage to the top electrodes as well as a small part of the membrane. The areas labeled A, B, and C are the locations where the Raman spectroscopy data in Fig. 4(c) are taken. Raman spectroscopy is performed at room temperature in ambient conditions.

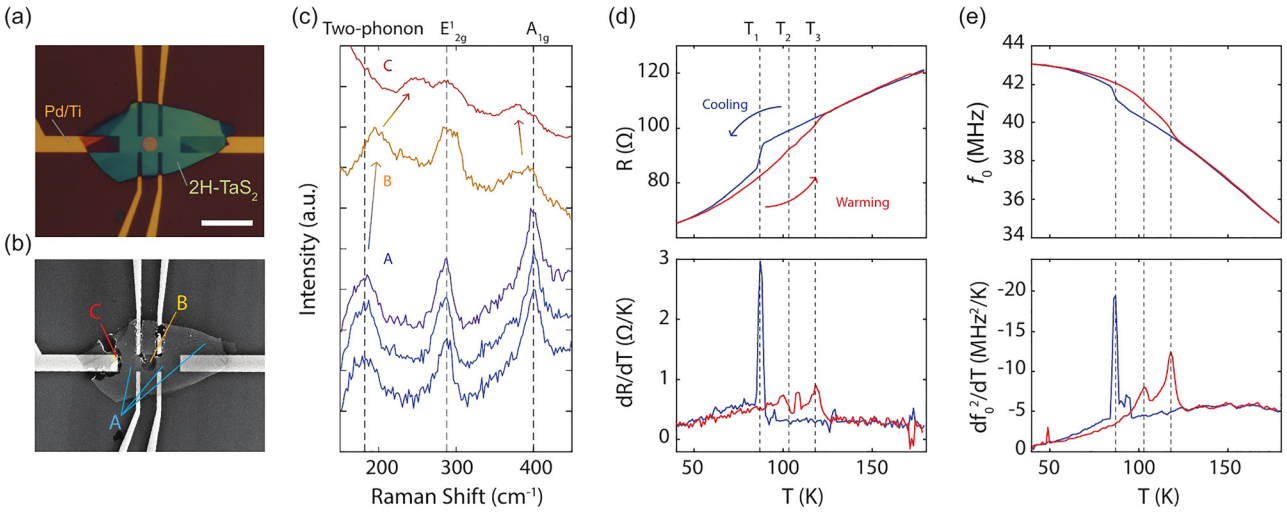

FIG. 4. Raman, electrical, and mechanical characterizations of device 4 (2H-TaS_2) showing competing transitions of CDW with an enhanced T_{CDW}. (a) Optical image of device 4 immediately after the fabrication. Scale bar: 10 μm. (b) SEM image of device 4 after the measurement. Labels A, B, and C indicate the positions where Raman spectroscopy data were acquired. (c) Raman spectroscopy data at A, B, and C. Dashed lines indicate the position of two-phonon mode, E^1_{2g} and A_{1g}. (d) Two-point resistance as a function of temperature (top) and its derivative (bottom). (e) Resonance frequency f_0 as a function of temperature (top) and $\frac{d[f_0^2(T)]}{dT}$ (bottom). In both (d) and (e), the blue lines indicate measurements taken while cooling down, and the red lines indicate measurements taken while warming up, as indicated by the arrows in (d). Dashed lines indicate the positions of the transition temperatures $T_1 = 87$ K, $T_2 = 103$ K, and $T_3 = 118$ K.

The blue Raman spectra shown in Fig. 4(c) are from the areas surrounding the drum and show the spectra comparable to literature.[17,52] The three characteristic peaks of 2H-TaS_2 are plotted in dashed gray lines at 180 cm^{-1}, 286 cm^{-1}, and 400 cm^{-1} corresponding to the two-phonon mode, the in-plane E^1_{2g} mode, and the out-of-plane A_{1g} mode, respectively.[4] The yellow line in Fig. 4(c) is the Raman spectrum taken directly on the drum and shows slight red shifting of the two-phonon mode. The red line is the spectrum taken from the area with the most damage observed. This spectrum shows the most severely red shifted two-phonon mode as well as slightly blue shifted A_{1g} mode as indicated by the arrows.

Figure 4(d) shows the two-probe resistance—measured across the two wide electrodes far left and right of the cavity—of this device measured as a function of temperature (top) and its temperature derivative (bottom). The mechanical resonance of the membrane as a function of temperature (top) as well as $\frac{d[f_0]^2}{dT}$ (bottom) are plotted in Fig. 4(e). In both resistance and mechanics measurements, more than one phase transition accompanied by a hysteretic behavior in the temperature sweeps are observed. The red lines correspond to the measurements performed while warming up, and the blue lines to the measurements performed while cooling down. There are three distinct peaks in the $\frac{d[f_0^2(T)]}{dT}$ at $T_1 = 87$ K, $T_2 = 103$ K, and $T_3 = 118$ K. Between the lowest transition temperature and the highest, both the resistance and the mechanical resonance show hysteretic behavior of split branches in the R–T and the f_0–T data. Even though the effective area probed via transport and nanomechanics are not identical, similar behaviors are observed in both R–T and f_0–T, suggesting that the degraded area has a significant contribution to the resistance as well as the mechanics. This experiment has been repeated multiple times to rule out measurement artifacts, but nonetheless, the hysteresis was present every time.

We believe that both the thickness and degradation are playing a role in our observation of enhanced T_{CDW} in Figs. 3 and 4. The study by Bekaert *et al.*[20] on the "healing" of the sulfur vacancies by oxygen demonstrated that the electron–phonon coupling could be enhanced by 80%, thus increasing the T_{SC}. Also, Zhang *et al.* recently reported the persistence of the CDW up to 140 K in the monolayer.[18] The increase in T_{CDW} upto 129 K in our air degraded sample could be an indication of partial amorphization of the multilayer sample, which reduces the effective thickness of the crystal from bulk toward an intermediate, few-effective-layers.

The two-phonon mode shown in Fig. 4(c) represents a second-order scattering process, where an electron scatters to create a pair of phonons with opposite momenta near the CDW wave vector q_{CDW}.[3] Softening of the two-phonon peaks below T_{CDW} in many 2H-MX_2 systems has been observed and used to characterize the CDW.[4,52–56] Typically, the position of the two-phonon mode shifts down with decreasing temperature, and the peak disappears as it reaches the CDW state. This is a direct result of the phonon dispersion renormalization due to the Kohn anomaly forming at T_{CDW}. The fact that we see differences in the two-phonon mode, and the out of plane A_{1g} mode in the degraded areas is indicative of local changes in the phonon branches and the chemical bond lengths caused by degradation. Controlled systematic Raman study of degradation dynamics should be conducted to correlate the changes in the chemical bonds to the phonon dispersion relation and the T_{CDW}.

The enhancement of the T_{CDW} from the nominal 75 K up to 118 K in Fig. 4 may be due to a degradation similar to the one observed in Fig. 3 but is attributed in this case to the discharge which caused the flake and the electrodes to be damaged. The absence of the peaks at 103 K and 118 K in the downward sweep and at 87 K in the upward sweep may be an indication of competition between various domains with different transition temperatures. This picture is further supported by the difference in the Raman spectra taken at room temperature in various areas of the same flake.

In conclusion, we studied the CDW transitions in the archetypal vdW systems 2H-TaS_2 and 2H-$TaSe_2$, by using the resonance frequency of suspended membranes. The temperature dependence of the resonance frequency can be translated into the specific heat, which shows an anomaly at the phase transition temperature. We showed that the degradation can irreversibly change the CDW transition temperature from the nominal value of $T_{CDW} = 75$ K to as high as 129 K. Furthermore, we studied a suspended drum with a partial local disorder which showed multiple transition temperatures as well as a hysteresis loop. In this work, we have demonstrated that the nanomechanical resonance is a powerful tool to study the CDW transitions in ultrathin-suspended vdW materials complementary to the temperature-dependent electronic transport.

See the supplementary material for methods (S.I), derivation of free energy and specific heat (S.II), additional data on the enhancement of CDW by exposure to air (S.III), and additional methods of inducing disorder explored (S.IV).

AUTHORS' CONTRIBUTIONS

M.L. and M.Š. contributed equally to this work.

M.L., M.Š., P.G.S., and H.S.J.v.d.Z. acknowledge funding from the European Union's Horizon 2020 research and innovation program under Grant Agreement No. 881603. E.C. and S.M.-V. acknowledge the financial support from the European Union (ERC AdG Mol-2D No. 788222), the Spanish MICINN (No. MAT2017–89993-R and Excellence Unit "María de Maeztu," No. CEX2019–000919-M), and the Generalitat Valenciana (PO FEDER Program, Nos. IDIFEDER/2018/061 and PROMETEO).

DATA AVAILABILITY

The data that support the findings of this study are openly available in Zenodo at https://doi.org/10.5281/zenodo.4719865, Ref. 57.

REFERENCES

[1] J. A. Wilson, F. D. Salvo, and S. Mahajan, "Charge-density waves and superlattices in the metallic layered transition metal dichalcogenides," Adv. Phys. **24**(2), 117–201 (1975).
[2] J. C. Tsang, J. E. Smith, Jr., and M. W. Shafer, "Raman spectroscopy of soft modes at the charge-density-wave phase transition in 2H-$NbSe_2$," Phys. Rev. Lett. **37**(21), 1407 (1976).
[3] S. Sugai, "Lattice vibrations in the charge-density-wave states of layered transition metal dichalcogenides," Phys. Status Solidi B **129**(1), 13–39 (1985).
[4] S. Sugai, K. Murase, S. Uchida, and S. Tanaka, "Studies of lattice dynamics in 2H-TaS_2 by Raman scattering," Solid State Commun. **40**(4), 399–401 (1981).
[5] J. M. E. Harper, T. H. Geballe, and F. J. Di Salvo, "Heat capacity of 2H-$NbSe_2$ at the charge density wave transition," Phys. Lett. A **54**(1), 27–28 (1975).

[6]R. A. Craven and S. F. Meyer, "Specific heat and resistivity near the charge-density-wave phase transitions in 2H-$TaSe_2$ and 2H-TaS_2," Phys. Rev. B **16**(10), 4583 (1977).
[7]R. Delaplace, P. Molinie, and D. Jerome, "On the pressure dependence of a charge density wave state in 2H-TaS_2," J. Phys. Lett. **37**(1), 13–15 (1976).
[8]T. M. Rice and G. K. Scott, "New mechanism for a charge density wave instability," Phys. Rev. Lett. **35**(2), 120 (1975).
[9]G. Campagnoli, A. Gustinetti, A. Stella, and E. Tosatti, "Plasmon behavior at the charge density wave onset in 2H-$TaSe_2$," Phys. Rev. B **20**(6), 2217 (1979).
[10]E. F. Steigmeier, G. Harbeke, H. Auderset, and F. J. Di Salvo, "Softening of charge density wave excitations at the superstructure transition in 2H-$TaSe_2$," Solid State Commun. **20**(7), 667–671 (1976).
[11]J. C. Tsang, J. E. J. Smith, M. W. Shafer, and S. F. Meyer, "Raman spectroscopy of the charge-density-wave state in 1T-and 2H-$TaSe_2$," Phys. Rev. B **16**(4239), 4239 (1977).
[12]W. L. McMillan, "Theory of discommensurations and the commensurate-incommensurate charge-density-wave phase transition," Phys. Rev. B **14**(4), 1496 (1976).
[13]D. E. Moncton, J. D. Axe, and F. J. Di Salvo, "Neutron scattering study of the charge density wave transitions in 2H-$TaSe_2$ and 2H-$NbSe_2$," Phys. Rev. B **16**(2), 801 (1977).
[14]J. A. Wilson, "Questions concerning the form taken by the charge density wave and the accompanying periodic structural distortions in 2H-$TaSe_2$ and closely related materials," Phys. Rev. B **17**(10), 3880 (1978).
[15]X. Xi, L. Zhao, Z. Wang, H. Berger, L. Forró, J. Shan, and K. F. Mak, "Strongly enhanced charge-density-wave order in monolayer $NbSe_2$," Nat. Nanotechnol. **10**(9), 765–769 (2015).
[16]C. Sergio, M. R. Sinko, D. P. Gopalan, N. Sivadas, K. L. Seyler, K. Watanabe, T. Taniguchi, A. W. Tsen, X. Xu, D. Xiao, and B. M. Hunt, "Tuning ising superconductivity with layer and spin–orbit coupling in two-dimensional transition-metal dichalcogenides," Nat. Commun. **9**(1), 1427 (2018).
[17]E. Navarro-Moratalla, J. O. Island, S. Manas-Valero, E. Pinilla-Cienfuegos, A. Castellanos-Gomez, J. Quereda, G. Rubio-Bollinger, L. Chirolli, J. A. Silva-Guillén, N. Agraït, G. A. Steele, F. Guinea, H. S. J. van der Zant, and E. Coronado, "Enhanced superconductivity in atomically thin TaS_2," Nat. Commun. **7**(1), 11043 (2016).
[18]D. Zhang, Y. Wu, Y.-H. Su, M.-C. Hsu, C. Ó Coileáin, J. Cho, M. Choi, B. S. Chun, Y. Guo, C.-R. Chang, and H.-C. Wu, "Charge density waves and degenerate modes in exfoliated monolayer 2H-TaS_2," IUCrJ **7**(5), 913–919 (2020).
[19]Y. Wu, J. He, J. Liu, H. Xing, Z. Mao, and Y. Liu, "Dimensional reduction and ionic gating induced enhancement of superconductivity in atomically thin crystals of 2H-$TaSe_2$," Nanotechnology **30**(3), 035702 (2019).
[20]J. Bekaert, E. Khestanova, D. G. Hopkinson, J. Birkbeck, N. Clark, M. Zhu, D. A. Bandurin, R. Gorbachev, S. Fairclough, Y. Zou, M. Hamer, D. J. Terry, J. J. P. Peters, A. M. Sanchez, B. Partoens, S. J. Haigh, V. Milošević, V. Milorad, and I. Grigorieva, "Enhanced superconductivity in few-layer TaS_2 due to healing by oxygenation," Nano Lett. **20**(5), 3808–3818 (2020).
[21]R. Yang, W. Luo, S. Chi, D. Bonn, and G. M. Xia, "The stability of exfolicated FeSe nanosheets during in-air device fabrication processes," IEEE Trans. Nanotechnol. **18**, 37–41 (2019).
[22]K. S. Novoselov, D. Jiang, F. Schedin, T. J. Booth, V. V. Khotkevich, S. V. Morozov, and A. K. Geim, "Two-dimensional atomic crystals," Proc. Natl. Acad. Sci. **102**(30), 10451–10453 (2005).
[23]L. J. Sandilands, A. A. Reijnders, A. H. Su, V. Baydina, Z. Xu, A. Yang, G. Gu, T. Pedersen, F. Borondics, and K. S. Burch, "Origin of the insulating state in exfoliated high-T_c two-dimensional atomic crystals," Phys. Rev. B **90**(8), 081402 (2014).
[24]Y. Yu, L. Ma, P. Cai, R. Zhong, C. Ye, J. Shen, G. D. Gu, X. H. Chen, and Y. Zhang, "High-temperature superconductivity in monolayer $Bi_2Sr_2CaCu_2O_{8+\delta}$," Nature **575**(7781), 156–163 (2019).
[25]L. D. Landau and E. M. Lifshitz, *Course of Theoretical Physics*, Statistical Physics Vol. 5 (Pergamon Press, 1968).
[26]E. B. Nyeanchi, D. F. Brewer, T. E. Hargreaves, A. L. Thomson, C. Liezhao, and C. Zhao-Jia, "The specific heat of BSCCO (2201) single crystal at low temperatures," Physica C: Supercond. **235**, 1755–1756 (1994).
[27]Y. Takano, N. Arai, A. Arai, Y. Takahashi, K. Takase, and K. Sekizawa, "Magnetic properties and specific heat of MPS_3 (M = Mn, Fe, Zn)," J. Magn. Magn. Mater. **272–276**, E593–E595 (2004).
[28]L. R. Testardi, "Elastic modulus, thermal expansion and specific heat at a phase transition," Phys. Rev. B **12**(9), 3849 (1975).
[29]J. W. Loram, J. L. Tallon, and W. Y. Liang, "Absence of gross static inhomogeneity in cuprate superconductors," Phys. Rev. B **69**(6), 060502 (2004).
[30]S. V. Grabovsky, I. V. Shnaidshtein, M. Takesada, A. Onodera, and B. A. Strukov, "Calorimetric study of ferroelectric $BaTiO_3$ in cubic phase," J. Adv. Dielectr. **3**(4), 1350032 (2013).
[31]M. Šiškins, M. Lee, S. Mañas-Valero, E. Coronado, Y. M. Blanter, H. S. van der Zant, and P. G. Steeneken, "Magnetic and electronic phase transitions probed by nanomechanical resonators," Nat. Commun. **11**(1), 2698 (2020).
[32]D. Davidovikj, D. J. Groenendijk, A. M. R. Monteiro, A. Dijkhoff, D. Afanasiev, M. Šiškins, M. Lee, Y. Huang, E. van Heumen, H. S. J. van der Zant, A. D. Caviglia, and P. G. Steeneken, "Ultrathin complex oxide nanomechanical resonators," Commun. Phys. **3**(1), 163 (2020).
[33]S. Jiang, H. Xie, J. Shan, and K. F. Mak, "Exchange magnetostriction in two-dimensional antiferromagnets," Nat. Mater. **19**(12), 1295–1299 (2020).
[34]S. Sengupta, H. S. Solanki, V. Singh, S. Dhara, and M. M. Deshmukh, "Electromechanical resonators as probes of the charge density wave transition at the nanoscale in $NbSe_2$," Phys. Rev. B **82**(15), 155432 (2010).
[35]A. Castellanos-Gomez, M. Buscema, R. Molenaar, V. Singh, L. Janssen, H. S. Van Der Zant, and G. A. Steele, "Deterministic transfer of two-dimensional materials by all-dry viscoelastic stamping," 2D Mater. **1**(1), 011002 (2014).
[36]D. C. Freitas, P. Rodière, M. R. Osorio, E. Navarro-Moratalla, N. M. Nemes, V. G. Tissen, L. Cario, E. Coronado, M. García-Hernández, S. Vieira, M. Núñez Regueiro, and H. Suderow, "Strong enhancement of superconductivity at high pressures within the charge-density-wave states of 2H-TaS_2 and 2H-$TaSe_2$," Phys. Rev. B **93**(18), 184512 (2016).
[37]M. Saint-Paul and P. Monceau, "Survey of the thermodynamic properties of the charge density wave systems," Adv. Condens. Matter Phys. **2019**, 1.
[38]G. K. White, J. A. Birch, and M. H. Manghnani, "Thermal properties of sodium silicate glasses at low temperatures," J. Non-Cryst. Solids **23**(1), 99–110 (1977).
[39]K. G. Lyon, G. L. Salinger, C. A. Swenson, and G. K. White, "Linear thermal expansion measurements on silicon from 6 to 340 K," J. Appl. Phys. **48**(3), 865–868 (1977).
[40]M. Barmatz, L. R. Testardi, and F. J. Di Salvo, "Elasticity measurements in the layered dichalcogenides $TaSe_2$ and $NbSe_2$," Phys. Rev. B **12**(10), 4367 (1975).
[41]D. Lin, S. Li, J. Wen, H. Berger, L. Forró, H. Zhou, S. Jia, T. Taniguchi, K. Watanabe, X. Xi, and M. S. Bahramy, "Patterns and driving forces of dimensionality-dependent charge density waves in 2H-type transition metal dichalcogenides," Nat. Commun. **11**(1), 2406 (2020).
[42]J. W. Jiang and Y. P. Zhou, "Parameterization of stillinger-weber potential for two-dimensional atomic crystals," arXiv:1704.03147 (2017).
[43]J. Kang, S. Tongay, J. Zhou, J. Li, and J. Wu, "Band offsets and heterostructures of two-dimensional semiconductors," Appl. Phys. Lett. **102**(1), 012111 (2013).
[44]D. S. Sanditov and V. N. Belomestnykh, "Relation between the parameters of the elasticity theory and averaged bulk modulus of solids," Tech. Phys. **56**(11), 1619–1623 (2011).
[45]T. Middelmann, A. Walkov, G. Bartl, and R. Schödel, "Thermal expansion coefficient of single-crystal silicon from 7 K to 293 K," Phys. Rev. B **92**(17), 174113 (2015).
[46]F. Hao, X. Liao, M. Li, H. Xiao, and X. Chen, "Oxidation-induced negative Poisson's ratio of phosphorene," J. Phys.: Condens. Matter **30**(31), 315302 (2018).
[47]A. Falin, M. Holwill, H. Lv, W. Gan, J. Cheng, R. Zhang, D. Qian, M. R. Barnett, E. J. Santos, K. S. Novoselov, and T. Tao, "Mechanical properties of atomically thin tungsten dichalcogenides: WS_2, WSe_2, and WTe_2," ACS Nano **15**(2), 2600–2610 (2021).
[48]Q. Li, Q. Zhou, L. Shi, Q. Chen, and J. Wang, "Recent advances in oxidation and degradation mechanisms of ultrathin 2D materials under ambient conditions and their passivation strategies," J. Mater. Chem. A **7**(9), 4291–4312 (2019).
[49]M. T. Lavik, T. M. Medved, and G. D. Moore, "Oxidation characteristics of MoS_2 and other solid lubricants," ASLE Trans. **11**(1), 44–55 (1968).
[50]S. J. Cartamil-Bueno, P. G. Steeneken, F. D. Tichelaar, E. Navarro-Moratalla, W. J. Venstra, R. van Leeuwen, E. Coronado, H. S. van der Zant, G. A. Steele, and A. Castellanos-Gomez, "High-quality-factor tantalum oxide

nanomechanical resonators by laser oxidation of $TaSe_2$," Nano Res. **8**(9), 2842–2849 (2015).
[51]I. E. Rosłoń, R. J. Dolleman, H. Licona, M. Lee, M. Šiškins, H. Lebius, L. Madauß, M. Schleberger, F. Alijani, H. S. J. van der Zant, and P. G. Steeneken, "High-frequency gas effusion through nanopores in suspended graphene," Nat. Commun. **11**(1), 6025 (2020).
[52]K. Zhang, Z.-Y. Cao, and X.-J. Chen, "Effects of charge-density-wave phase transition on electrical transport and Raman spectra in 2H-tantalum disulfide," Appl. Phys. Lett. **114**(14), 141901 (2019).
[53]P. Hajiyev, C. Cong, C. Qiu, and T. Yu, "Contrast and Raman spectroscopy study of single-and few-layered charge density wave material: 2H-$TaSe_2$," Sci. Rep. **3**(1), 1–6 (2013).
[54]J. Joshi, H. M. Hill, S. Chowdhury, C. D. Malliakas, F. Tavazza, U. Chatterjee, A. R. H. Walker, and P. M. Vora, "Short-range charge density wave order in 2H-TaS_2," Phys. Rev. B **99**(24), 245144 (2019).
[55]J. Pandey and A. Soni, "Electron-phonon interactions and two-phonon modes associated with charge density wave in single crystalline 1T-VSe_2," Phys. Rev. Res. **2**(3), 033118 (2020).
[56]M. Klein, "Theory of two-phonon Raman scattering in transition metals and compounds," Phys. Rev. B **24**(8), 4208 (1981).
[57]M. Lee, M. Šiškins, S. Mañas-Valero, E. Coronado, P. G. Steeneken, and H. S. J. van der Zant (2021). "Study of charge density waves in suspended 2H-TaS2 and 2H-TaSe2 by nanomechanical resonance," Zenodo. https://doi.org/10.5281/zenodo.4719865